Electronic structure of $Pr_{1-x}Y_xBa_2Cu_3O_y$ ($x=0$, 0.5, and 1.0)

Katsuyoshi Kakinuma and Kazuo Fueki
Department of Industrial Chemistry, Faculty of Science and Technology, Science University of Tokyo, Yamazaki, Noda-shi, Chiba 278, Japan

(Received 11 December 1996; revised manuscript received 7 April 1997)

In order to elucidate the reason why $PrBa_2Cu_3O_y$ is not a superconductor, we examined the Pr valence and measured the oxygen nonstoichiometry and the conductivity at temperatures up to 1200 K for three kinds of oxides, $PrBa_2Cu_3O_y$, $(Pr_{0.5}Y_{0.5})Ba_2Cu_3O_y$, and $YBa_2Cu_3O_y$. The valence of Pr was found to be +3. Any difference was not found in oxygen nonstoichiometry and conductivity among three kinds of oxides. We analyzed the data of oxygen nonstoichiometry on the basis of defect thermodynamics and calculated the numbers of Cu^+, Cu^{2+}, and Cu^{3+} ions in the unit cell as a function of y. The number of Cu^{3+} ions (the amount of holes) was found to be proportional to $(\Delta y)^{1.6}(\Delta y=y-6.0)$, whereas the conductivity was found to be proportional to $(\Delta y)^{3.2}$ in these oxides. We interpreted the remarkable increase of σ with Δy as an evidence of the increase of both mobility and hole concentration with Δy. At high temperatures, we detected the conductivity minimum $\sigma_{\min}$ which was found in the $\log_{10}\sigma-\log_{10}P_{O_2}$ plot at constant temperatures. From the slope of the Arrhenius plot for $\sigma_{\min}$, the band gap was determined to be 1.21, 1.32, and 1.37 eV for $PrBa_2Cu_3O_y$, $(Pr_{0.5}Y_{0.5})Ba_2Cu_3O_y$ and $YBa_2Cu_3O_y$, respectively. We determined the conductivity of the same oxygen content as a function of temperature from 4.2 to 1200 K. The energy gap ΔE between the acceptor level and the top of the valence band was calculated from the slope of the Arrhenius plot for conductivity. ΔE for superconducting $YBa_2Cu_3O_y$ and $(Pr_{0.5}Y_{0.5})Ba_2Cu_3O_y$ were zero at 300 K but that for nonsuperconducting $PrBa_2Cu_3O_y$ was 20 meV at 100 K even for $y=6.93$. It was concluded that the conductivity of the high-temperature superconducting oxide was found to be strongly dependent on the defects and was explained using the semiconducting model which was introduced by the impurity level of excess oxygen. Namely, the existence of the energy gap ΔE causes the remarkable decrease in carrier density with decreasing temperature and results in the nonsuperconduction of $PrBa_2Cu_3O_y$. [S0163-1829(97)04530-X]

I. INTRODUCTION

Shortly after the discovery of the high transition temperature in $YBa_2Cu_3O_y$, other superconductors of the 90-K class were found by substituting Y^{3+} with rare-earth ions in $YBa_2Cu_3O_y$.[1–3] Most rare-earth ions give 90-K superconductors. Only the Ce, Tb, Pm, and Pr rare-earth ions do not. For Ce, Tb, and Pm the reason is clear. Indeed, Ce and Tb do not form the 123 oxide and Pm is radioactive and unstable. In contrast, $PrBa_2Cu_3O_y$ is a stable 123 oxide with the same crystal structure as $YBa_2Cu_3O_y$ and undergoes the structural tetragonal to orthorhombic transition when the oxygen content is increased. So the reason why $PrBa_2Cu_3O_y$ is not a superconductor, in spite of its resemblance to $YBa_2Cu_3O_y$, attracted much attention.[4–6] By the conductivity and Hall coefficient measurements, it was found that in $PrBa_2Cu_3O_y$ the carrier density is lower than in $YBa_2Cu_3O_y$.[7–10] This is understood to arise from the hole trapping, which is occurred by the existence of a Pr^{4+} ion in $PrBa_2Cu_3O_y$. But the valence in $PrBa_2Cu_3O_y$ is still unclear. The calculation of the bond valence sum[11] gave an average valence between 3.1 and 3.4. The magnetic susceptibility measurement[12] yielded 3.87 of the Pr ion. But the results of x-ray absorption spectroscopy[13] (XAS) and electron-energy-loss spectroscopy[14] (EELS) is +3. Different experiments concluded different valences for the Pr ion in $PrBa_2Cu_3O_y$. Therefore, hole trapping could not be concluded to be the reason why $PrBa_2Cu_3O_y$ is not a superconductor. Further, it has been argued that pair breaking[15,16] occurs due to the presence of Pr^{3+}. According to this theory, the $4f$ electrons in the Pr^{3+} ion interact with the spins of the CuO_2 plane at the Fermi level suppressing the superconductivity. Indeed, the neutron inelastic-scattering experiment[17–20] has shown that the peaks of $PrBa_2Cu_3O_y$ are broad whereas those of $YBa_2Cu_3O_y$ are sharp. The broadening observed for $PrBa_2Cu_3O_y$ could arise from the interaction of Pr^{3+} with the CuO_2 spins. But it could not be certified and, at present, the reason why $PrBa_2Cu_3O_y$ is not a superconductor has not been clarified yet.

A different approach was used in the present study. In general, the electrical conduction of a metal oxide depends on the oxygen nonstoichiometry. When the oxide is stoichiometric, it is an insulator. With increasing deviation from stoichiometry, the oxide becomes more electroconductive. The oxides with oxygen excess (metal deficit) are of *p* type, because the excess oxygen plays the role of acceptor and produces holes in the valence band. On the other hand, the oxides with oxygen deficit (metal excess) are *n* type, because the metallic ion of the lower valence plays the role of donor and creates conduction electrons in the conduction band. High-temperature superconductors have large oxygen nonstoichiometry and most of them have an excess of oxygen. Therefore, they are *p* type. Only a few superconducting oxides, such as $(Nd_{1-x}Ce_x)_2CuO_4$ and $(Sm_{1-x}Ce_x)_2CuO_4$, are *n* type and have conduction electrons. It has been verified that the critical temperature (T_c) is closely related to the

oxygen nonstoichiometry. Accordingly, for the superconducting oxides, useful information about the occurrence of superconductivity in the oxide can be obtained from the variation of their physical properties as a function of the oxygen nonstoichiometry. For this reason, we investigated the oxygen dependency of conductivity at low and high temperatures, which yields information on the carrier density and mechanism of the carrier formation.

Superconductivity occurs at low temperatures, but the samples are usually annealed at a high temperature and then quenched down to low temperatures. For example, $(La_{1-x}Ba_x)_2CuO_4$ $(0.04 \leqslant x \leqslant 0.07)$ is a thermodynamic instability below room temperature.[21,22] When this sample is quenched at low temperature, it changes from a stable superconducting low temperature orthorhombic phase to instable semiconducting low temperature tetragonal phase. In this phase transition occurs anomalies of conductivity and critical temperature in this system. This anomaly is called the 1/8 anomaly. Therefore, at first, the oxygen nonstoichiometry and conductivity are investigated at high temperatures, because the equilibrium is easily established and reproducible results can be obtained. The data at high temperature are useful as a reference for the interpretation of the low-temperature properties.

Finally, we determine the band gap (CT gap) and the gap between the acceptor level and valence band using the conductivity minimum $\sigma_{\min}$ and the p-type conductivity. From these results, we propose the model of electronic structure which uses the acceptor level of excess oxygen in order to interpret why $PrBa_2Cu_3O_y$ is not a superconductor.

II. EXPERIMENT

A. Sample preparation

Homogeneous samples were obtained with the coprecipitation method, i.e., by mixing 0.5-mol/l aqueous solutions of $Pr(NO_3)_3$, $Y(NO_3)_3$, and $Cu(NO_3)_2$ and 0.25-mol/l $Ba(NO_3)_2$ solutions in the desired ratio. The concentrations of these solutions were determined by the method of chelate titration. Oxalic acid was weighted 1.5 times more than metal ions in equivalent measures and was dissolved in ethanol, which has four times larger volume than the mixed aqueous solution. The oxalic-acid–ethanol solution was mixed with the prepared aqueous solution to coprecipitate metal oxalates. The pH was adjusted at 3. After aging for one night, the precipitate was filtrated, dried at 100 °C for several hours, and finally decomposed into oxides at 400 °C. Calcination was made at 850 °C for 24 h in air to form 123 oxide. $PrBa_2Cu_3O_y$ powder was pressed into pellets at 400 kgf/cm^2 and sintered at 935 °C for 24 h in air. The sintered body was ground in an agate mortar, and the powder was pressed and sintered at 935 °C for 48 h in air again. In the case of $YBa_2Cu_3O_y$ and $Pr_{0.5}Y_{0.5}Ba_2Cu_3O_y$, a first sintering was made at 950 °C for 24 h in an oxygen atmosphere. After being pressed into a pellet, a second sintering was made at 950 °C for 36 h in an oxygen atmosphere.

B. Chemical analysis

The metal composition was determined by the method of ICP (inductively coupled plasma) spectroscopy (Seiko SPS-7000). The valence of Pr and the average valence of Pr+Cu were determined using the method of chlorine evolution[23] along with iodmetry.

C. Measurement of oxygen content

The oxygen content has been determined at high temperatures as a function of the oxygen partial pressure using a microbalance (TGA-41, Shimadzu) equipped with a gas system. A powder sample of each kind of oxide was annealed at 300 °C or 350 °C for 48 h in air. The oxygen content of these samples was determined by iodmetry. Next, about 0.5 g of sample was weighed, put in a platinum basket and suspended from the beam of the balance. The first reading was employed as the reference weight. The weight change was measured from the reference as a function of oxygen partial pressure and temperature. From the result, the oxygen content y was calculated. The measurement was made in temperatures between 300 °C and 800 °C for $PrBa_2Cu_3O_y$ and in temperatures between 350 °C and 1000 °C for $Pr_{0.5}Y_{0.5}Ba_2Cu_3O_y$ and $YBa_2Cu_3O_y$. The oxygen partial pressure ranging from 1.0 to 1.0×10^{-4} atm was adopted.

D. Measurement of the conductivity

A powder sample was pressed into a disk and then sintered. The inner sintered pellet of each kind of oxide was observed by a SEM to check for porosity. The Archimedes method using benzene as a medium gave densities 5.97, 6.19, and 6.33 g/ cm^3 for $YBa_2Cu_3O_{6.93}$, $Pr_{0.5}Y_{0.5}Ba_2Cu_3O_{6.93}$, and $PrBa_2Cu_3O_{6.93}$, respectively. The pellet of each kind of oxide was cut into a rectangular shape (10 mm × 5 mm × 0.5 mm). Generally, the stoichiometric metal oxide is an insulator, the metal deficit (in the case of oxygen excess) oxide is a p-type one and the metal excess (in the case of oxygen deficit) oxide is an n-type one. When the oxygen partial pressure P_{O_2} is increased at high temperatures, the semiconducting property of metal oxide changes from an n type to a p type and the minimum ($\sigma_{\min}$) of conductivity appears. From the Arrhenius plot for $\sigma_{\min}$, the band gap (CT gap) is determined. For this purpose, the high-temperature conductivity has been determined as a function of oxygen partial pressure at constant temperatures by four Pt electrodes. The oxygen partial pressure has been adjusted by the mixing ratio of oxygen and argon and checked with an oxygen sensor. The conductivity between 4.2 and 523 K was measured using the sintered pellet which was controlled oxygen content by an annealing technique. The oxygen content was determined by iodmetry using powder taken from the same batch and annealed under the same condition as the pellet.

III. RESULTS AND DISCUSSION

A. Chemical analysis

The metal composition was determined by the method of ICP spectrometry. For three kinds of oxides, the compositions were Pr:Ba:Cu=1.00:2.00:3.00, Pr:Y:Ba:Cu =0.50:0.50:2.00:3.00, and Y:Ba:Cu=1.00:2.00:3.00. Trace of Cl_2, which indicated the existence of Pr^{4+} in the $PrBa_2Cu_3O_y$, was not detected. It was concluded that the Pr valence is +3.

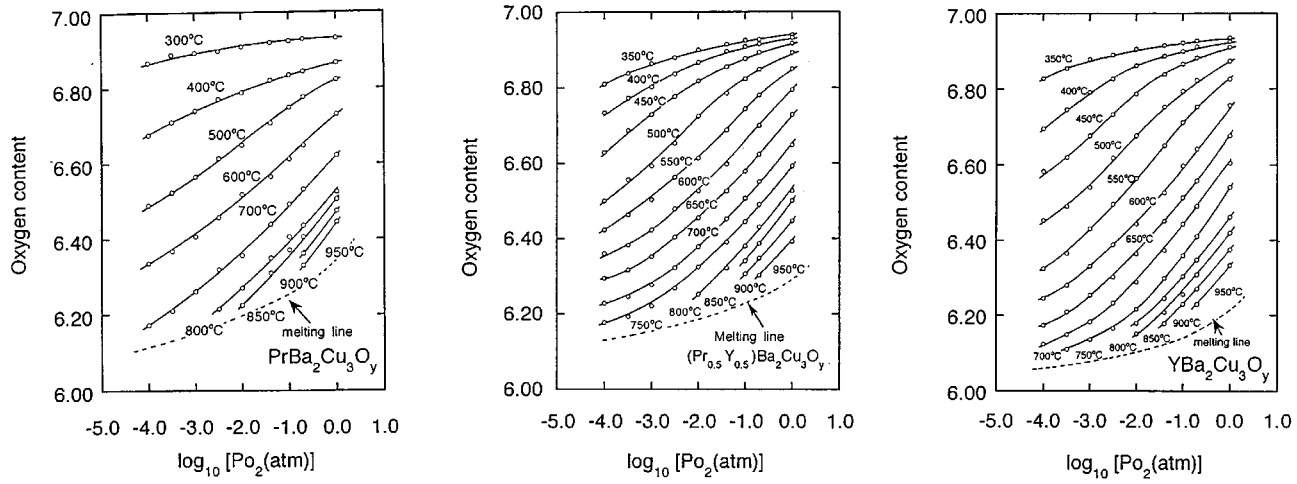

FIG. 1. Oxygen content as a function of temperature and oxygen partial pressure.

B. Oxygen nonstoichiometry

The oxygen content was determined as a function of the oxygen partial pressure at constant temperature. Figure 1 shows the result for $PrBa_2Cu_3O_y$, $Pr_{0.5}Y_{0.5}Ba_2Cu_3O_y$, and $YBa_2Cu_3O_y$, respectively. It took 6 h to reach equilibrium, after we changed the oxygen pressure stepwise. The maximum oxygen content for the three oxides was 6.93. The present result for $YBa_2Cu_3O_y$ is in agreement with those of Kishio *et al.*,[24,25] but contrasts with the results[26,27] obtained by the scanning method using a TGA apparatus. This can be understood by the fact that the present method is an equilibrium procedure while the scanning method is not. Our result for $PrBa_2Cu_3O_y$ are almost same from those of Lindermer *et al.*[28]

The master curve[29,30] is obtained when the partial molar enthalpy of oxygen ($\Delta\overline{H}_{O_2}$)is independent of the oxygen content y. For $PrBa_2Cu_3O_y$, the master curve is obtained by taking the y-$\log_{10}P_{O_2}$curve for 600 °C (Fig. 1) as a reference, and shifting the other y-$\log_{10}P_{O_2}$ curves horizontally, i.e., parallel to the $\log_{10}P_{O_2}$ axis, towards the curve for 600 °C. Then, all the data points fall on a single curve, as is shown in Fig. 2. Similarly, the master curves for $Pr_{0.5}Y_{0.5}Ba_2Cu_3O_y$ and $YBa_2Cu_3O_y$ were achieved from the data shown in Fig. 2, respectively. The analysis of the master curve yields the numbers of Cu^+, Cu^{2+}, and Cu^{3+} ions in unit cells of three oxides. The result is shown in Fig. 3. The detail of the calculation is given in the Appendix. The number of Cu^+ ions decreases whereas that of Cu^{3+} increases with increasing oxygen content. The number of Cu^{2+} forms a convex curve with a maximum at $y=6.5$. The $[Cu^{3+}]$ vs y curve for $PrBa_2Cu_3O_y$ is almost the same as those for $Pr_{0.5}Y_{0.5}Ba_2Cu_3O_y$ and $YBa_2Cu_3O_y$. Similarly, the $[Cu^+]$ vs y curve is nearly the same for three kinds of oxides.

C. Conductivity

1. High-temperature conductivity

The authors and their coinvestigators have already shown that the electrical conductivity of high-temperature superconductors is closely related to the oxygen nonstoichiometry.[32–41] In this study, the high-temperature conductivity has been determined as a function of the oxygen partial pressure and temperature. The results are shown in Fig. 4 in a $\log_{10}\sigma$-$\log_{10}P_{O_2}$ plot. The curve of $YBa_2Cu_3O_y$ is in agreement with the results of Leonidov *et al.*[42] and by Grader *et al.*[43] We connected Fig. 4 with Fig. 1 and showed the result in Fig. 5 as plots of σ vs y. The data points for each oxide fall on a single curve, independent of temperature. This fact indicates that the high-temperature conductivity depends on the oxygen content but it is independent of temperature. A similar result of $YBa_2Cu_3O_y$ has been reported by Yoo *et al.*[44] The conductivity of $PrBa_2Cu_3O_y$ was found to be quite similar to the results of $Pr_{0.5}Y_{0.5}Ba_2Cu_3O_y$ and $YBa_2Cu_3O_y$. These conductivities seem to become zero as the oxygen content y approaches 6.0. Comparing Fig. 5 with Fig. 3, it was found that the conduction was mainly caused by holes, while the conduction of electrons was relatively small. Probably, the mobility of electrons is small compared to the one of holes. So far, measurements of high-temperature conductivity at constant oxygen partial pressures were reported by several investigators.[45–47] As seen in Fig. 1, the oxygen content of the oxides varies with temperature even when the oxygen partial pressure is kept constant. Therefore, the conductivity measured at constant oxygen partial pressure reflects the conductivity of different substances, i.e., different oxygen contents. Consequently, it was difficult to discuss the electrical properties in detail from the last conductivity data taken at constant oxygen partial pressure.

In Fig. 6, we show the $\log_{10}$-$\log_{10}$ plots of σ, $[Cu^{3+}]$, and the mobility calculated by $\sigma/([Cu^{3+}]\cdot e)$, against Δy $(=y-6.0)$ for the three kinds of oxides. The plots are linear over most of the part of the oxygen content range, with slopes from 3.1 to 3.3. Near $y=7.0$, the slopes increase to 3.9 to 4.1. The plots are straight and the slopes range from 1.5 to 1.7. Near $y=7.0$, the slope increases from 2.1 to 2.3. The slope of the $\log_{10}\sigma$-$\log_{10}\Delta y$ plot is higher than that of the $\log_{10}[Cu^{3+}]$ vs $\log_{10}\Delta y$ plot. We find that the mobility depends on the number of excess oxygen, i.e., the number of holes. The strong dependence of mobility on carrier concentration seems to be the characteristic feature of high-T_c superconductors in a normal state, because the carrier concen-

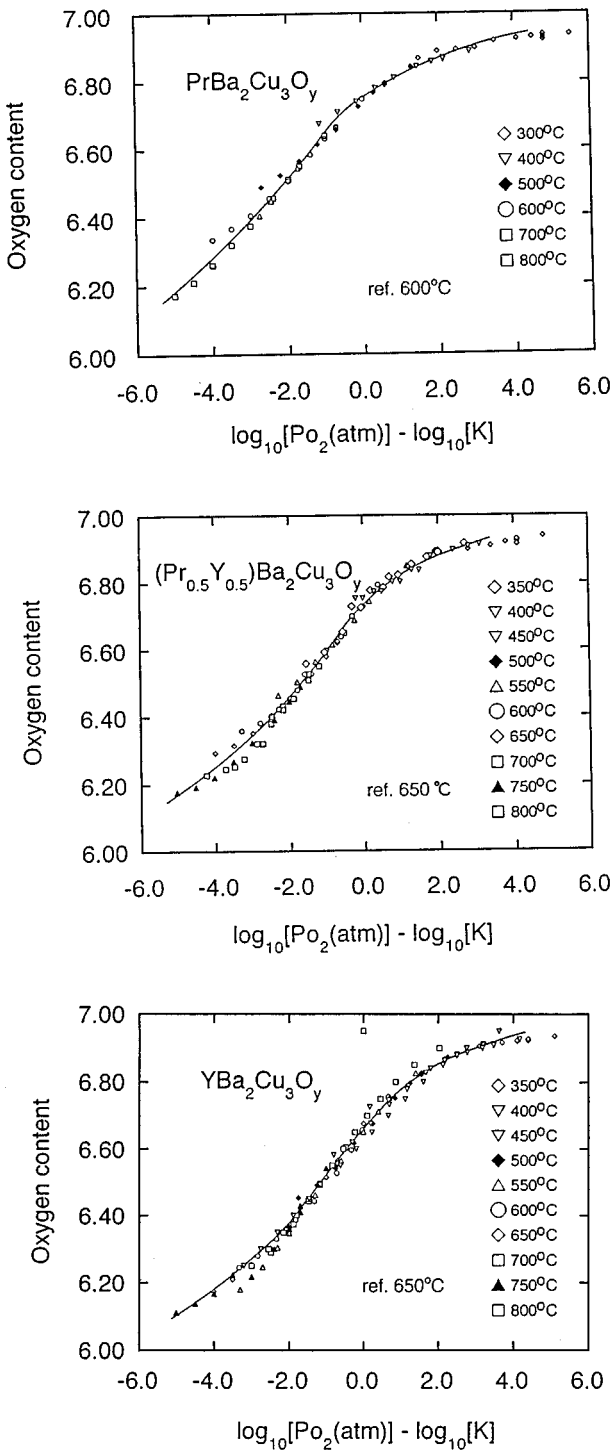

FIG. 2. Plot of oxygen content vs $\log_{10}P_{O_2}-\log_{10}K$.

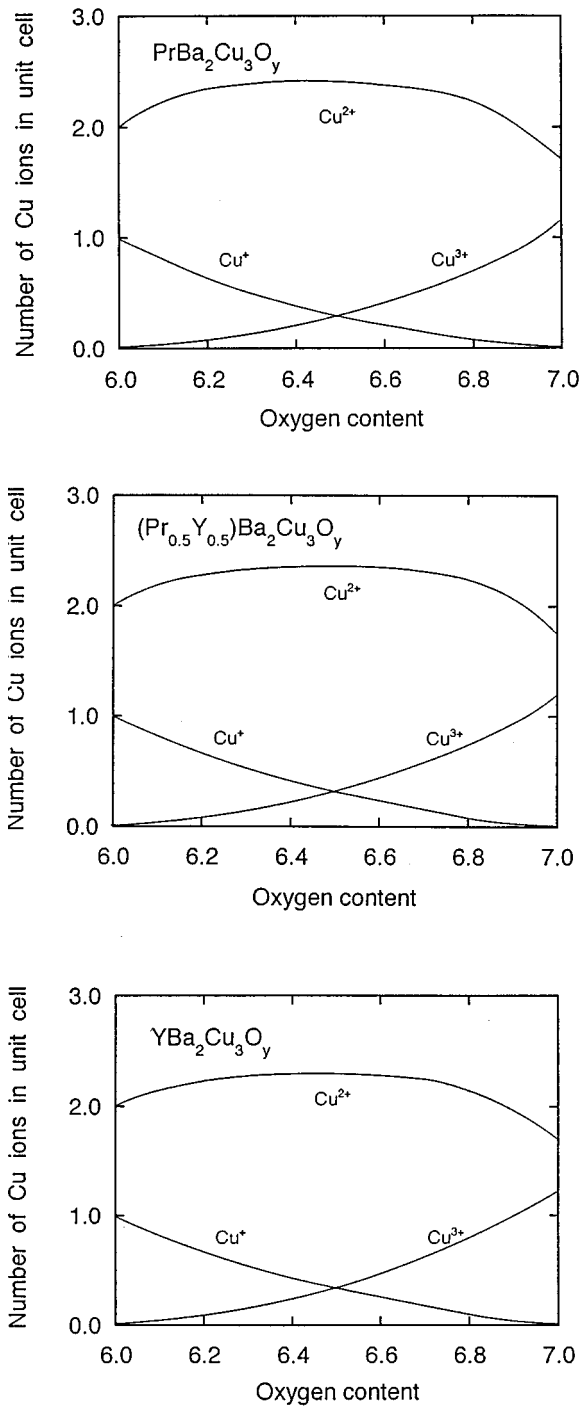

FIG. 3. Numbers of Cu^+, Cu^{2+}, and Cu^{3+} ions in a unit cell as a function of oxygen content. Equilibrium constants were listed in Table I.

tration is 3 orders of magnitude higher than usual semiconductors.

2. Temperature dependence of conductivity in a wide temperature range

Since the conductivity strongly depends on the oxygen content, the conductivity was studied as a function of oxygen content and temperature in the high- and low-temperature ranges. Figure 7 shows the temperature dependence of conductivity of $PrBa_2Cu_3O_y$, $(Pr_{0.5})Y_{0.5}Ba_2Cu_3O_y$, and $YBa_2Cu_3O_y$, respectively. The dotted lines above 573 K represent the conductivity at constant oxygen partial pressures. The solid lines above 573 K are the conductivity at constant oxygen contents, constructed by the combination of y-$\log_{10}P_{O_2}$ and σ-$\log_{10}P_{O_2}$ relations in Figs. 1 and 4. The conductivity below 573 K was measured by samples with controlled oxygen content. In particular, during the measurement of conductivity from 300 to 573 K, we checked that absorption and desorption of oxygen do not occur. The broken lines between 573 and 625 K are the connection between high- and low-temperature data. The high-temperature con-

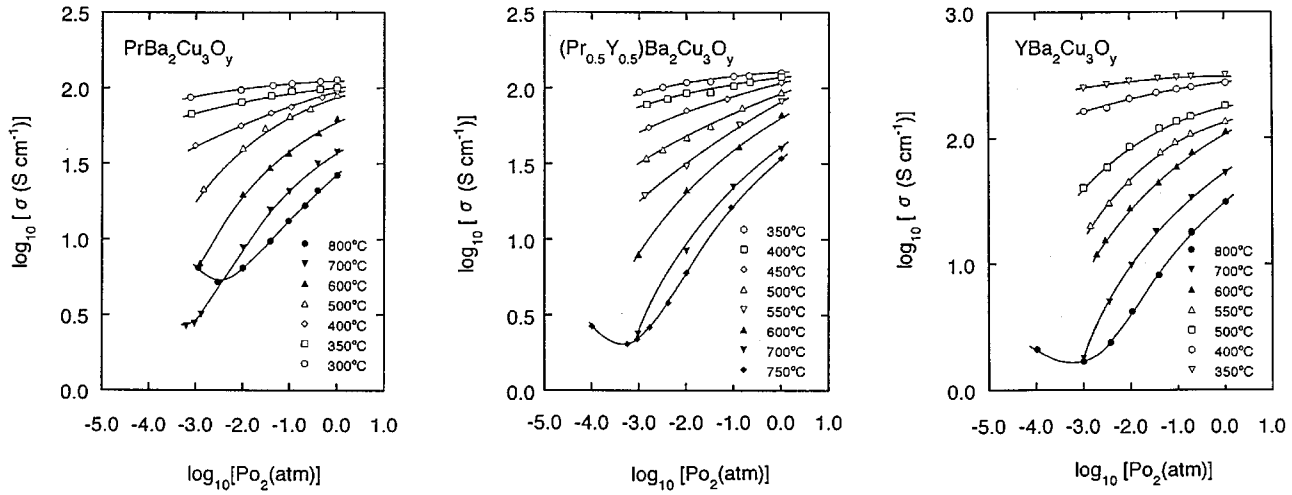

FIG. 4. Plot of $\log_{10}\sigma$ vs $\log_{10}P_{O_2}$.

ductivity is smoothly linked with the low-temperature one of the same oxygen content and is independent of temperature. As described in Fig. 5, the high-temperature conductivity is nearly independent of temperature. The fact indicates that both carrier density and mobility are independent on temperature. Leonidov *et al.* determined the high-temperature conductivity at constant oxygen content by changing the oxygen partial pressure.[48] They reported that the conductivity minimum was observed at 600 °C to 750 °C for $YBa_2Cu_3O_y$ with oxygen content smaller than 6.7, which was attributed to the change in transport mode. However, such a minimum was not observed in the present work. It is considered that the method by Leonidov *et al.* has been difficult in keeping the oxygen content constant. Freitas *et al.* determined the conductivity of $YBa_2Cu_3O_y$ by sweeping the temperature at a rate of 0.1–0.5 K/min.[49,50] Utilizing the oxygen content data by Jorgensen[51] they obtained the dependence of conductivity at constant oxygen content. According to them, the conductivity is independent of temperature when $y>6.6$, while it increases with increasing temperature when $y<6.6$. In the present study, the independence of conductivity on temperature has been observed even when y is 6.4. Probably, the difference between two results would be due to the method of measurement. It seems that the equilibrium method employed in the present study is more accurate than the sweep method employed by Freitas *et al.* for the determination of conductivity as a function of oxygen content. Comparison of Fig. 6 shows that the conductivities of $PrBa_2Cu_3O_y$ and $YBa_2Cu_3O_y$ above 600 K are nearly the same when the oxygen content is the same. However, with decreasing temperature, the conductivity of $YBa_2Cu_3O_y$ increases while that of $PrBa_2Cu_3O_y$ decreases remarkably. The conductivity of $(Pr_{0.5}Y_{0.5})Ba_2Cu_3O_y$ shows the intermediate temperature dependence between $YBa_2Cu_3O_y$ and $PrBa_2Cu_3O_y$. From the result, it is concluded that the nonsuperconducting characteristics of $PrBa_2Cu_3O_y$ are due to the remarkable decrease in conductivity below 600–700 K.

D. Carrier density and mobility

The carrier density of semiconductors, such as Si, is usually determined by the measurement of the Hall coefficient. Although the determination of carrier density from the Hall coefficient was tried on high- T_c superconductors shortly after the discovery,[52–56] the reproducibility of data was poor until the present time. One cause is the poor quality of the sample. Since the carrier density of oxides is governed by the oxygen nonstoichiometry as well as the metal composition, fine control of composition and accurate chemical analysis are required to obtain good quality. The second cause is limitation of the Hall coefficient measurement. Namely, the carrier density of high-T_c superconductors is on the order of 10^{21} cm^{-3} and is 10^2-10^3 times larger than that of semiconductors, such as doped Si. This fact means that the Hall coefficient of superconductors is 10^2—10^3 times smaller than that of semiconductors. The data of high accuracy are rather difficult to attain. Accordingly, in this study the carrier density and mobility are calculated from the conductivity and the content of excess oxygen. The majority carrier of $PrBa_2Cu_3O_y$, $(Pr_{0.5}Y_{0.5})Ba_2Cu_3O_y$, and $YBa_2Cu_3O_y$ is hole when y is larger than 6.2. At high temperatures, the conduc-

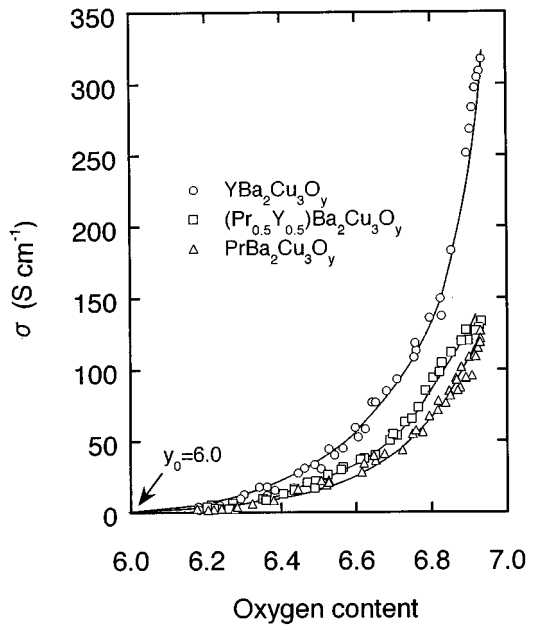

FIG. 5. Plots of σ vs oxygen content at high temperature.

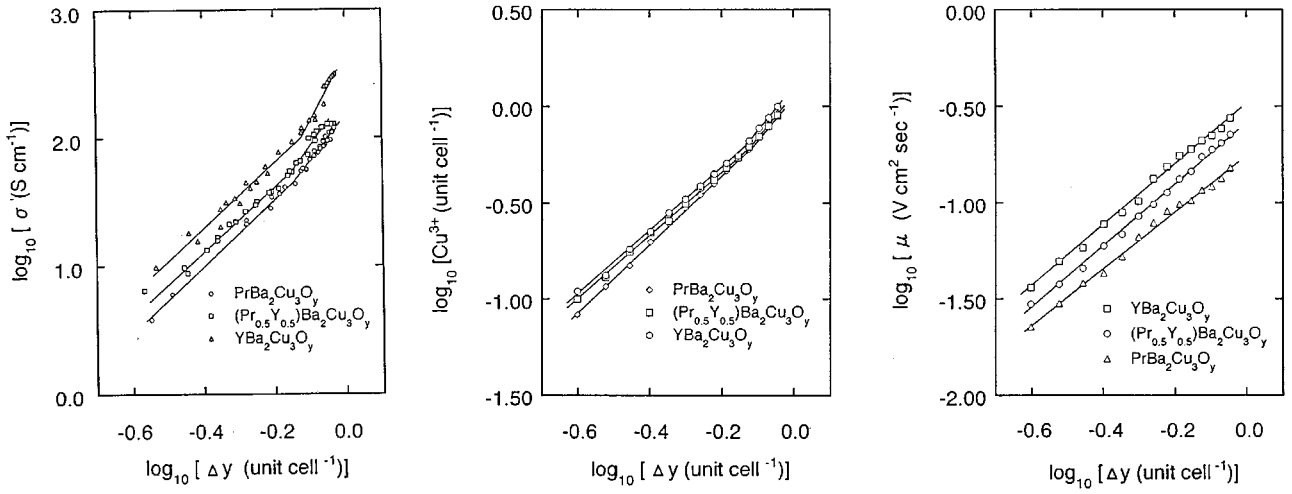

FIG. 6. Plots of $\log_{10}\sigma$, $\log_{10}[\Delta Cu^{3+}]$, and $\log_{10}\mu$ vs $\log_{10}[\Delta y]$ at high temperature.

tivity of these oxides is temperature independent as seen in Figs. 5 and 7. This fact indicates that both carrier density and mobility are temperature independent. Using the number of holes in a unit cell $[Cu^{3+}]$ and the lattice constants a, b, and c obtained in a previous paper, the carrier density is calculated by

$$n=\frac{[Cu^{3+}]}{abc}. \tag{1}$$

At low temperatures, the negative temperature coefficient of conductivity, namely the metal-like behavior, is observed for $(Pr_{0.5}Y_{0.5})Ba_2Cu_3O_y$ and $YBa_2Cu_3O_y$ when y is large. The temperature dependence of the conductivity is well interpreted as the increase of mobility with decreasing temperature at constant carrier density, rather than the increase of carrier concentration. The carrier concentration was calculated assuming that the low-temperature carrier concentration is the same as the high-temperature one. In the case of $PrBa_2Cu_3O_y$ and the case where y in $(Pr_{0.5}Y_{0.5})Ba_2Cu_3O_y$ and $YBa_2Cu_3O_y$ is small, the temperature dependence of conductivity is positive, in other words, the conduction is semiconducting. Usually, the temperature dependence of the semiconduction is interpreted in terms of $\exp(-\Delta E/kT)$, where ΔE is the energy gap between acceptor level and the top of the valence band in the case of a p-type semiconductor. The term of $\exp\{-\Delta E/(kT)\}$ indicates that the carrier density and the conductivity tends to saturate as the temperature rises. Such a saturation is seen in Fig. 7. Accordingly, assuming that the mobility is constant, the carrier concentration n is calculated by

$$\frac{\sigma}{\sigma_0}=\frac{n}{n_0}, \tag{2}$$

where σ is the low-temperature conductivity corresponding to n, and σ_0 is the high-temperature conductivity corresponding to n_0. The mobility μ is calculated by

$$\mu=\frac{\sigma}{n\cdot e}, \tag{3}$$

where e is the elementary charge. The carrier density and mobility of three kinds of oxides are shown in Figs. 8 and 9. The carrier density of $YBa_2Cu_3O_y$ with y larger than 6.43 is constant over the whole temperature range, while that of

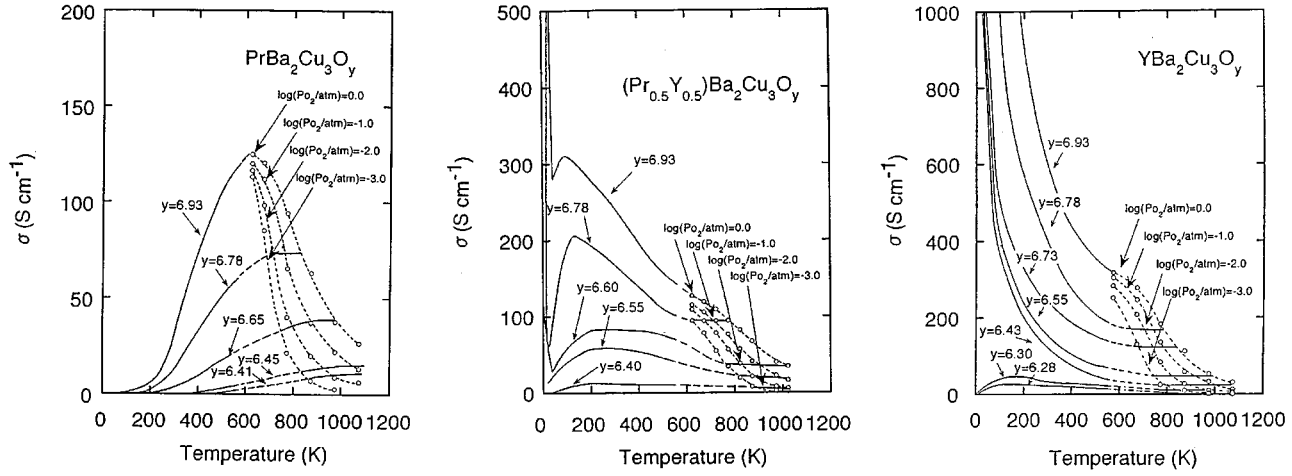

FIG. 7. Plot of conductivity vs temperature.

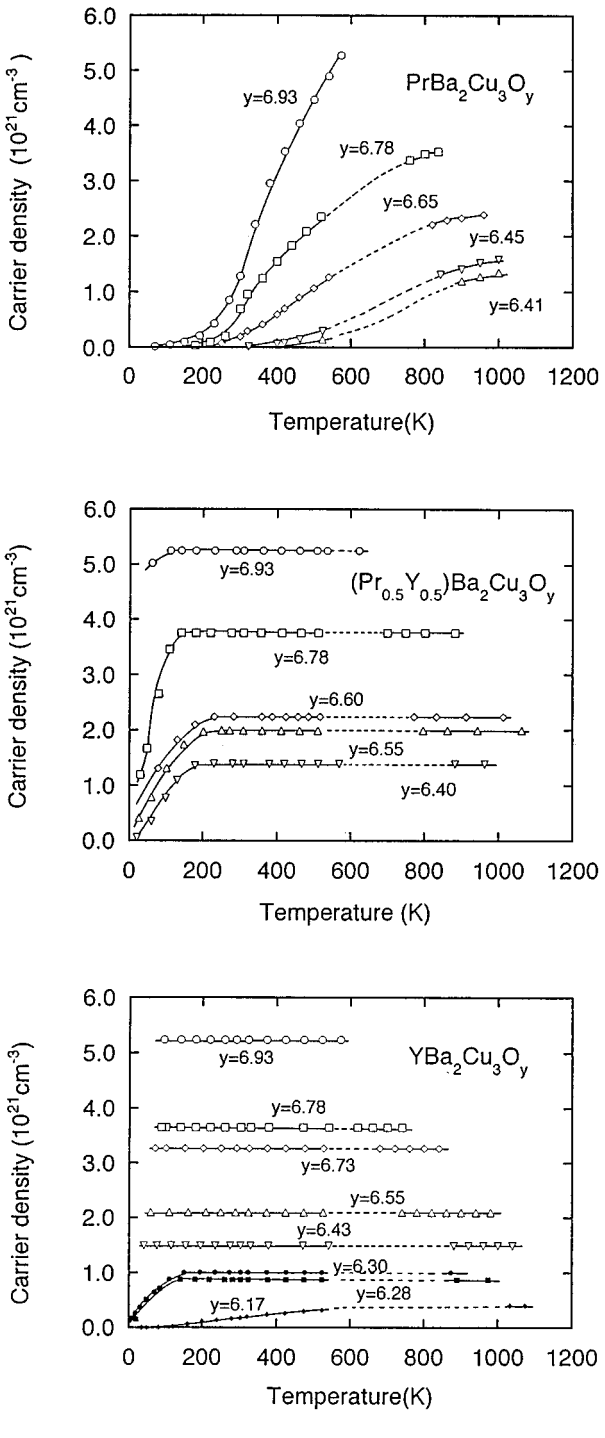

FIG. 8. Carrier density as a function of temperature.

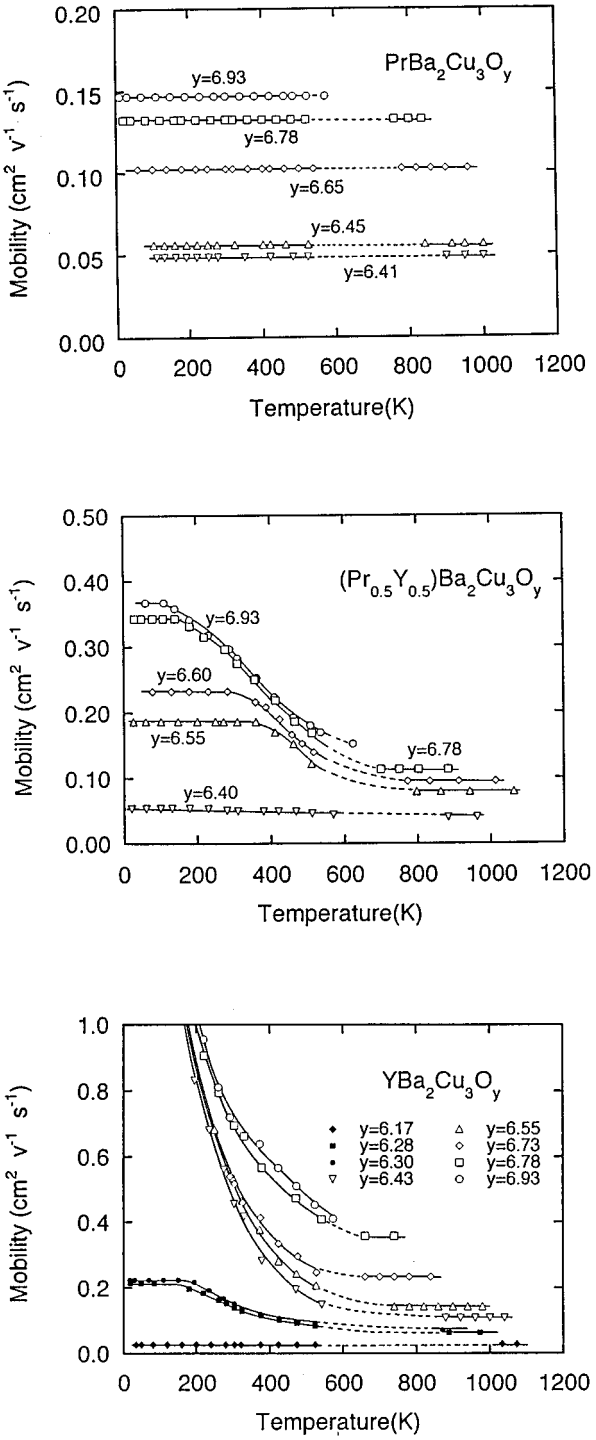

FIG. 9. Mobility as a function of temperature.

$PrBa_2Cu_3O_y$ decreases remarkably with decreasing temperature. The carrier density of $(Pr_{0.5}Y_{0.5})Ba_2Cu_3O_y$ decreases below 100–200 K. Summarizing these results, it is concluded that the carrier density of $PrBa_2Cu_3O_y$ is too low to form a Cooper pair even when oxygen content y is equal to 6.93. The Hall coefficient of $YBa_2Cu_3O_y$ has been measured by Yoo *et al.*[57] and of $PrBa_2Cu_3O_y$ by Parfinov *et al.*[58] respectively, at room temperature. The carrier density of $YBa_2Cu_3O_y$ calculated from the result is shown in Fig. 10 by open squares. For comparison, our result given in Fig. 8 is plotted in the same figure by open circles. Two results are very similar. A similar comparison of carrier density for $PrBa_2Cu_3O_y$ is shown in Fig. 10. Since the Hall voltage decreases with increasing carrier density, the accuracy of the Hall coefficient seems to decrease as the oxygen content increases. The mobility of $YBa_2Cu_3O_y$ with $y>6.4$ and $(Pr_{0.5}Y_{0.5})Ba_2Cu_3O_y$ with $y>6.8$ increases with lowering temperature and these oxides exhibit superconductivity. The mobility of $PrBa_2Cu_3O_y$ and nonsuperconducting $(Pr_{0.5}Y_{0.5})Ba_2Cu_3O_y$ and $YBa_2Cu_3O_y$ are 0.01–0.04 cm^2 V^{-1} s^{-1}.

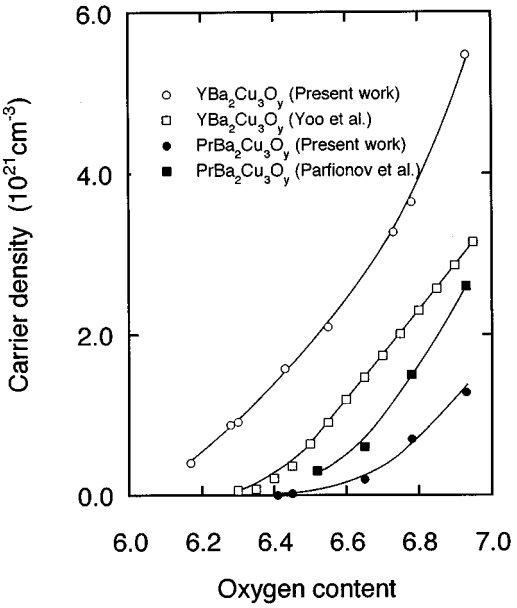

FIG. 10. Plot of carrier density vs oxygen content.

E. Electronic structure

1. Determination of CT gap from the conductivity minimum

When a metal deficit (oxygen excess) oxide is kept at high temperature and the oxygen partial pressure is raised, the oxide also absorbs oxygen, which dissociates into holes and oxide ion. The overall reaction is represented, for example,

$$O_2 \leftrightarrows 2O_i'' + 4h^+, \tag{4}$$

where O_i'' is interstitial divalent oxide ion and h^+ is a hole. Therefore, the metal-deficit oxide is essentially a p-type semiconductor. In the physical picture, the hole creation is interpreted as follows. The excess oxygen plays the role of acceptor, which is ionized to form holes in the valence band as a result of thermal excitation of electrons from the valence band to the acceptor level. The mass action law for Eq. (4) is

$$K_a = n_{(O_i'')^2} \cdot p^4. \tag{5}$$

$n_{(O_i'')}$ represents the concentration of interstitial oxygen ion, p is the hole density, P_{O_2} is the oxygen partial pressure, and K_a is the equilibrium constant. When the formation of defects represented by Eq. (4) is predominant,

$$2n_{(O_i'')} = p, \tag{6}$$

insertion of Eq. (6) into Eq. (5) yields

$$p \propto P_{O_2}^{1/6}. \tag{7}$$

Since the conductivity σ is proportional to p, σ is proportional to $P_{O_2}^{1/6}$. Generally, the conductivity of the metal-deficit oxide is proportional to $P_{O_2}^{1/\nu}$ where ν is characteristic of the mechanism of defect formation. Accordingly, the plot of $\log_{10}\sigma$-$\log_{10}P_{O_2}$ has a positive slope.

On the other hand, metal excess (oxygen-deficit) oxide loses oxygen and creates conduction electrons as the oxygen partial pressure is lowered. The reaction is represented, for example, by

$$2O^X \leftrightarrows O_2 + 2V_{\ddot{O}} + 4e^-, \tag{8}$$

where O^X represents oxide ion on the anion site, $V_{\ddot{O}}$ is the oxide ion vacancy and e^- is the conduction electron. Accordingly, the metal excess oxide is an n-type semiconductor. In the physical picture, the formation of conduction electrons are interpreted as follows. Loss of oxygen results in the formation of a lower valence metal ion, such as a Cu^+ ion in cuprate superconductors. Such a lower valence metal ion plays a role of donor and provides conduction electrons, for example, by such an excitation:

$$Cu^+ \leftrightarrows Cu^{2+} + e^-. \tag{9}$$

At high temperature, the chemical equilibrium given in Eq. (8) is easily reached. The mass action law is

$$P_{O_2} \cdot n_{(V_{\ddot{O}})}^2 \cdot n_e^4 = K_b, \tag{10}$$

where n_e is the density of conduction electrons. If the reaction (8) is predominant for the formation of defects,

$$n_{(V_{\ddot{O}})} = (1/2)n_e. \tag{11}$$

Insertion of Eq. (11) into Eq. (10) gives

$$P_{O_2} \cdot n_e^6 = \text{const.} \tag{12}$$

Accordingly

$$n_e \propto P_{O_2}^{-1/6}. \tag{13}$$

Generally, the conductivity of metal excess oxide is proportional to $P_{O_2}^{-1/\nu'}$ and ν' depends on the mechanism of defect formation. The plot of $\log_{10}\sigma$ vs $\log_{10}P_{O_2}$ has a negative slope. When the oxide has both the oxygen deficit and oxygen excess composition range, $\log_{10}\sigma$ changes the sign with increasing $\log_{10}P_{O_2}$ as shown in Fig. 11. The conductivity minimum $\sigma_{\min}$ appears in the middle of n-type and p-type regions, and

$$(1/2)\sigma_{\min} = \sigma_p = \sigma_n, \tag{14}$$

where σ_p and σ_n are conductivities due to holes and electrons, respectively. Denoting the mobilities of holes and electrons by μ_h and μ_e, we obtain

$$\sigma_p = pe\mu_h, \tag{15}$$

$$\sigma_n = ne\mu_e. \tag{16}$$

If $\mu_h = \mu_e$, n is equal to p at the conductivity minimum. The combination of Eq. (14) with Eqs. (15) and (16) yields

$$\{(1/2)\sigma_{\min}\}^2 = \sigma_p \cdot \sigma_n = (n \cdot p)e^2(\mu_h\mu_n). \tag{17}$$

If we represent the effective densities of state for conduction and valence bands by N_c and N_v, the band gap by E_g and the Boltzmann constant by k, respectively, we get

$$n \cdot p = N_c \cdot N_v \exp\{-E_g/(kT)\}. \tag{18}$$

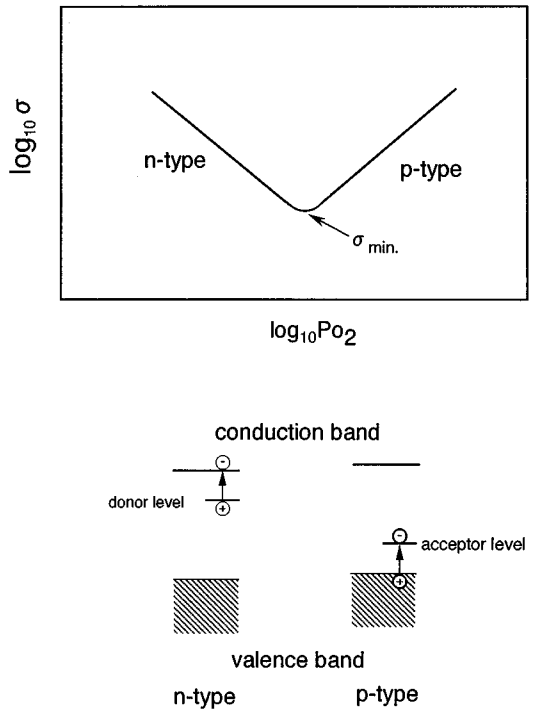

FIG. 11. Schematic drawing of $\log_{10}\sigma$ vs $\log_{10}P_{O_2}$ plot and electronic structure of metal oxides.

Insertion of Eq. (18) into Eq. (17) gives

$$\sigma_{\min}=2e(\mu_h\mu_n N_c N_v)^{1/2}\exp\{-E_g/(2kT)\}. \quad (19)$$

Accordingly,

$$\log_{10}\sigma_{\min}=\log_{10}\sigma_0-E_g/(2.303\cdot 2kT). \quad (20)$$

If μ_h and μ_n are temperature independent, we can determine the CT gap from the slpoe of the plot of $\log_{10}\sigma_{\min}$ vs $1/T$.[66]

The dependence of conductivity on oxygen partial pressure for $PrBa_2Cu_3O_y$, $(Pr_{0.5}Y_{0.5})Ba_2Cu_3O_y$, and $YBa_2Cu_3O_y$ is given in Fig. 12 and the Arrhenius plot for $\sigma_{\min}$ is given in Fig. 13, indicating a good linearity. As shown in Fig. 9, the mobility at high temperatures is independent of temperature. Therefore, from the slope of the Arrhenius plot one can determine the band gap, which is also given in Fig. 13. Although the CT gap becomes a little smaller as the Pr content increases, the gap for three kinds of oxides is considered to be nearly the same. As to the CT gap of high-T_c superconductors, the optical reflectivity measurement has given 1.5 eV for $YBa_2Cu_3O_y$,[59] 1.7–1.9 eV for $YBa_2Cu_3O_y$,[60] 2.0 eV for La_2CuO_4,[61–63] 1.2 eV for $(La_{1-x}Sr_x)_2CuO_4$,[64] and 1.5 eV for $Bi_2Sr_2Ca_{1-x}Y_xCu_2O_y$.[65] Most of the values are in a range 1.2–2.0 eV, which are in good agreement with the values given in Fig. 13. If μ_h is equal to μ_n, $\sigma_{\min}$ should appear at $y=6.5$, because n is equal to p at the oxygen content. However, $\sigma_{\min}$ for three kinds of oxides was found not at $y=6.5$ but at $y=6.2$, as μ_h is larger than μ_p. Equations (20) and (21) still hold in this case, and Eg can be determined.

2. Arrhenius plot of conductivity over the whole temperature range

Figures 4 and 11 indicate that the high-temperature superconductors are regarded as a kind of semiconductor doped with impurity, as well as other kinds of metal oxides. The temperature dependence of conductivity of a semiconductor containing a definite amount of dopant is schematically shown by I and II in Fig. 14. I is the case of low dopant concentration. With the temperature rise the conductivity increases in accordance with $\exp(-\Delta E/kT)$ as shown by I-(a). If the mobility is temperature independent, ΔE is the gap between the acceptor level E_a and top of the valence band E_v for the case of a p-type semiconductor and is the gap between the bottom of the conduction band E_c and donor level E_d for the case of an n-type semiconductor. In a high-temperature region where $kT>\Delta E$, the conductivity is constant irrespective of temperature, as shown by I-(b). In the extremely high-temperature region, the direct excitation of electrons from valence to conduction bands is predominant and the conductivity increases in accordance with $\exp\{-E_g/(2kT)\}$, as shown by I-(c). As the dopant concentration becomes high, ΔE becomes small. If ΔE is small enough compared to kT in a wide temperature range, the temperature-independent conductivity is observed as shown by II. The dependence represented by III is not found in the case of the semiconductor, but found in the case of the high-T_c superconductor which gives the T linear dependence of resistivity. the Arrhenius plots of conductivity for $PrBa_2Cu_3O_y$, $(Pr_{0.5}Y_{0.5})Ba_2Cu_3O_y$, and $YBa_2Cu_3O_y$ with constant y are given in Fig. 15. The broken line with open triangles on the left was transferred from Fig. 13. The plot of $PrBa_2Cu_3O_y$ is similar to I in Fig. 14. In $(Pr_{0.5}Y_{0.5})Ba_2Cu_3O_y$ and $YBa_2Cu_3O_y$, the plots for super-

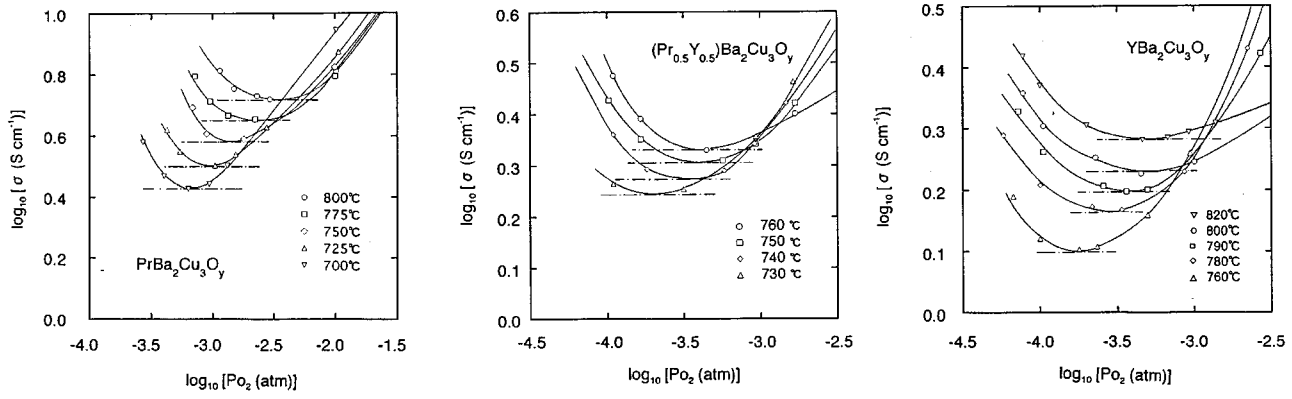

FIG. 12. Plot of $\log_{10}\sigma$ vs $\log_{10}P_{O_2}$. The dotted lines represented the tangent ones. Each $\sigma_{\min}$ was denoted by the point of contact.

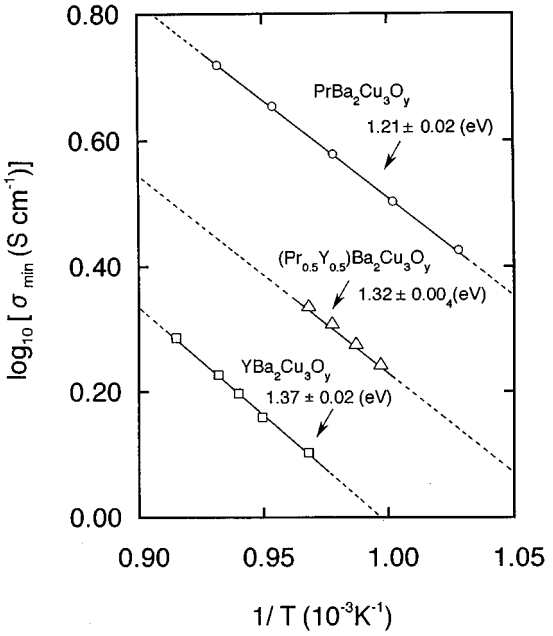

FIG. 13. Arrhenius plot for conductivity minimum $\sigma_{\min}$.

conduction are similar to I in Fig. 14, whereas the plots for superconductor are similar to II and III.

3. Electronic structure model

The gap ΔE between the acceptor level and the top of the valence band was roughly estimated from the slopes at 250 and 100 K of the Arrhenius plot for conductivity. The result is given in Fig. 16. The gap for each oxide decreases with the oxygen content. $\Delta E(100\ \mathrm{K})$ of $YBa_2Cu_3O_y$ becomes 0 at around $y=6.38$ above which the oxide becomes superconducting. When the oxygen content of $(Pr_{0.5}Y_{0.5})Ba_2Cu_3O_y$ is above 6.56, ΔE (100 K) becomes 0 as seen in Fig. 16. In the case of $PrBa_2Cu_3O_y$, $\Delta E(100\ \mathrm{K})$ is 100 meV higher than that of $YBa_2Cu_3O_y$ with the same y and is always positive over the whole oxygen content range. Therefore, $PrBa_2Cu_3O_y$ is nonsuperconducting. From the results of $\Delta E(100\ \mathrm{K})$ and E_g, the following electronic structure is proposed for $PrBa_2Cu_3O_y$, $(Pr_{0.5}Y_{0.5})Ba_2Cu_3O_y$, and $YBa_2Cu_3O_y$. When $(Pr_{0.5}Y_{0.5})Ba_2Cu_3O_y$ and $YBa_2Cu_3O_y$ are superconducting, the acceptor level originated from the

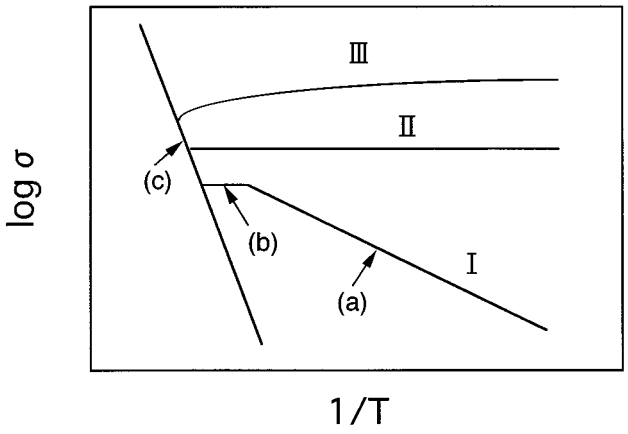

FIG. 14. Schematic drawing of the Arrhenius plot for conductivity.

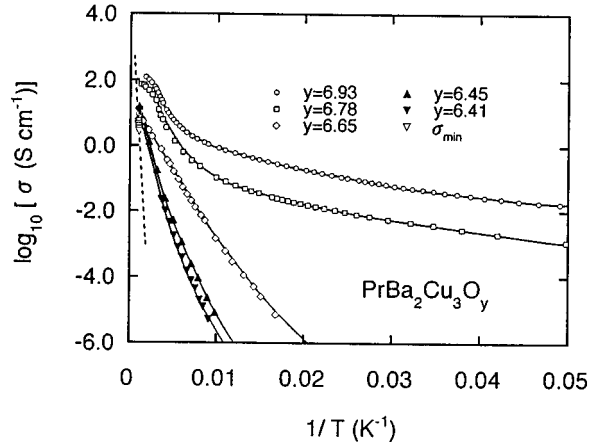

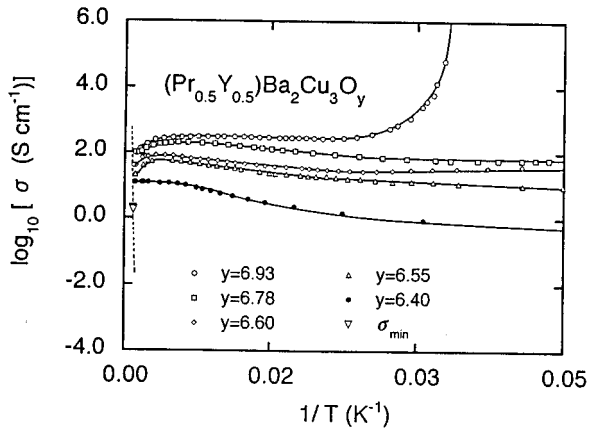

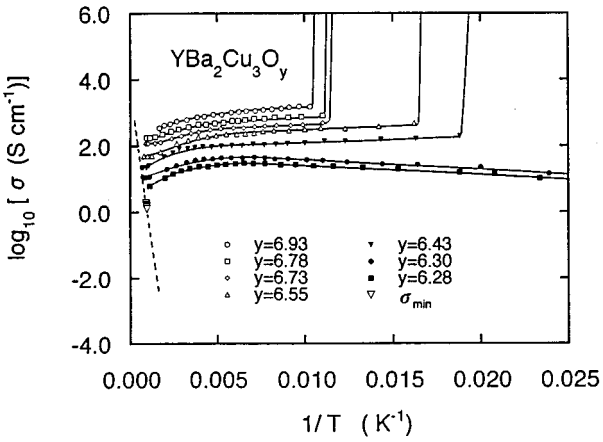

FIG. 15. Arrhenius plot for conductivity.

excess oxygen is incorporated into the valence band, as shown in Fig. 17(b). The excess oxygen is completely ionized to O^{2-}. Accordingly, the hole density is temperature independent and is high enough to form Cooper pairs. However, in the case of $PrBa_2Cu_3O_y$, ΔE is always positive, as shown in Fig. 17(a) over the whole range of oxygen content. Therefore, the density of holes in the valence band decreases with decreasing temperature. The hole concentration in the

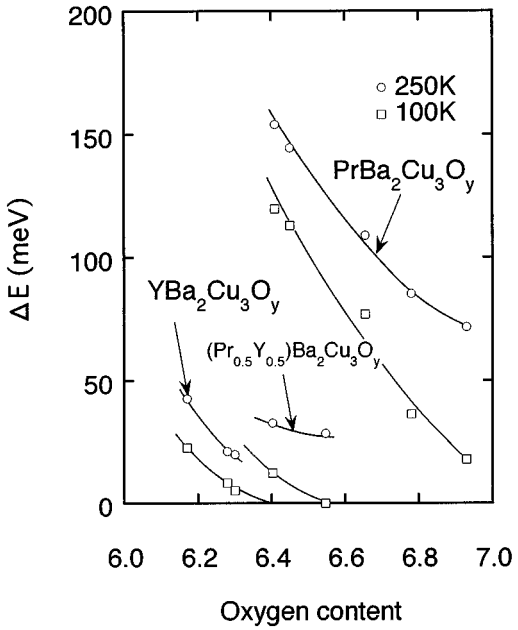

FIG. 16. Energy gap ΔE plotted against oxygen content.

valence band is too small to form Cooper pairs. Holes seem to reside not on Pr^{3+} ions but in the acceptor originated from the excess oxygen.

IV. DISCUSSION

On the basis of the results, we discuss the characteristic feature of conduction of high-T_c superconductors in a normal state. The conductivity of superconductors in a normal state is in a range from 10^2 to 10^3 S cm^{-1} and is located in the middle of a normal metal and semiconductor. Accordingly, there are two approaches for the elucidation of conduction. One is the approach from the normal metal and the other is that from a semiconductor. The first approach assumes the occurrence of a free carrier. To verify this, the optical conductivity has been calculated from the reflectivity using the Kramers-Krönig transformation. If free carriers exist, the plasma frequency determined from the Drude term should be proportional to the square root of carrier concentration. However, it has become apparent that the plasma frequency is independent of carrier concentration for most of the high-T_c superconductors in the normal state.[67] This fact seems not to support the occurrence of free carriers. We took the second approach, namely, the approach from the semiconductor, and the conduction was studied on three kinds of oxides, superconducting $YBa_2Cu_3O_y$, nonsuperconducting $PrBa_2Cu_3O_y$, and their intermediate $(Pr_{0.5}Y_{0.5})Ba_2Cu_3O_y$. The conductivity of the semiconductor containing a definite amount of dopant changes with the temperature rise. The temperature dependence of conductivity is classified into three regions, an impurity (extrinsic) one, an exhausting one, and an intrinsic one. $PrBa_2Cu_3O_{6.9}$ is a semiconductor and its conductivity rises steeply with increasing temperature and reaches the saturation at around 300 °C. This shows the switching over from the extrinsic region to the exhausting region. Superconducting oxides are always in the exhausting region. Moreover, the existence of the intrinsic region has been shown by the determination of E_g from $\sigma_{\min}$, though the intrinsic region is observed only in high-temperature and low oxygen pressure.

The excess oxygen is crucial to the high-T_c superconductor since it acts as the dopant. The increase in oxygen content enhances the conductivity, broadens the exhaustion region, and lowers the activation energy for conduction. If the exhaustion region extended to a temperature lower than T_c, the superconduction would appear. The only difference between a high-T_c superconductor and a usual semiconductor is the dependence of mobility on carrier concentration. The mobility of the usual semiconductor is considered to be independent on carrier concentration, but that of superconductors strongly depends on carrier concentration, as seen in Fig. 8. The origin of strong dependence is not clear at the present time. The interaction between carriers would be the cause, because the carrier concentration of superconductors is 2–3 orders of magnitude larger that of a semiconductor. The concentration-dependent mobility seems characteristic of a high-T_c superconductor. We summarize that the conducting property is interpreted by the semiconductor model in connection with the concentration-dependent mobility.

V. SUMMARY

From these data, it was found that the conductivity of $Pr_{1-x}Y_xBa_2Cu_3O_y$ ($x=0$, 0.5, and 1.0) was strongly dependent on an oxygen defect. So, we strictly controlled oxygen partial pressure, temperature, and oxygen content and measured the conductivity and oxygen nonstoichiometry of $PrBa_2Cu_3O_y$, $Pr_{0.5}Y_{0.5}Ba_2Cu_3O_y$, and $YBa_2Cu_3O_y$ for a wide range of temperature. From these data, we summarized the conclusion in seven sentences.

(1) The method of chlorine evolution indicates that the Pr

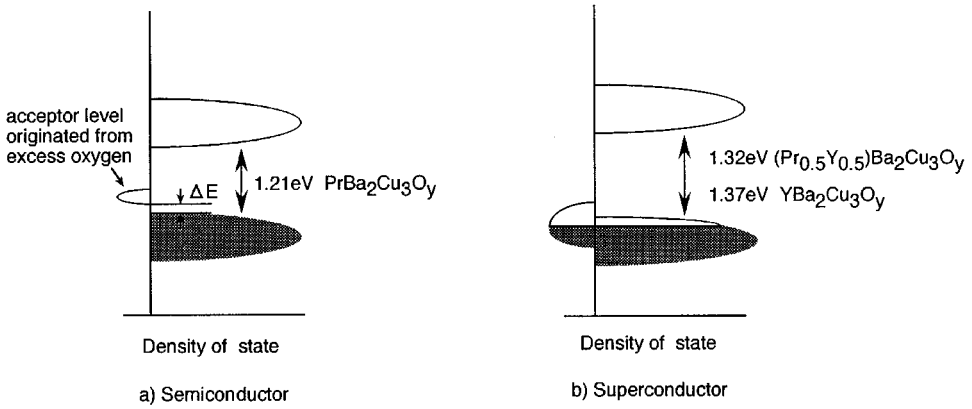

FIG. 17. Schematic drawing of the electronic structure of $(Pr_{1-x}Y_x)Ba_2Cu_3O_y$.

valence in $PrBa_2Cu_3O_y$ and $Pr_{0.5}Y_{0.5}Ba_2Cu_3O_y$ is $+3$.

(2) The oxygen content y of $PrBa_2Cu_3O_y$, $Pr_{0.5}Y_{0.5}Ba_2Cu_3O_y$, and $YBa_2Cu_3O_y$ was determined as a function of the oxygen partial pressure and temperature. It was found that y of the three oxides is nearly the same when the oxygen partial pressure and the temperature are the same.

(3) In high temperature, all the data points of σ vs Δy were found to fall on a single curve. It can be concluded that the high-temperature conductivity is independent of temperature. Moreover, $[Cu^{3+}]$ (hole concentration) and mobility are not dependent on temperature but on oxygen content.

(4) The CT gap was determined from the slope of the Arrhenius plot for $\sigma_{\min}$. The values of 1.21, 1.32, and 1.37 eV were found for $PrBa_2Cu_3O_y$, $(Pr_{0.5}Y_{0.5})Ba_2Cu_3O_y$, and $YBa_2Cu_3O_y$, respectively.

(5) The conductivity below 573 K was measured on three kinds of oxides with controlled oxygen content. The conductivity-temperature curve in a low-temperature range was smoothly linked with that in a high-temperature range, when the oxygen content was the same.

(6) The energy gap ΔE between the acceptor level and the top of the valence band was determined from the slope of Arrhenius plot of conductivity. $\Delta E(100\ \mathrm{K})$ decreased with increasing oxygen content y and become zero at $y=6.40$ for $YBa_2Cu_3O_y$ and at $y=6.55$ for $(Pr_{0.5}Y_{0.5})Ba_2Cu_3O_y$. In the higher oxygen content range, $\Delta E(100\ \mathrm{K})=0$ and the superconduction was observed. $\Delta E(100\ \mathrm{K})$ for $PrBa_2Cu_3O_y$ was always positive over the whole oxygen content range.

(7) On the basis of the results, an electronic structure based on the semiconductor model has been proposed.

I. APPENDIX: ANALYSIS OF THE MASTER CURVE

The analysis of the master curve yields information on both electronic and ionic defects. According to the calculation of he bond valence sum of Brown,[31] for the oxygen content ranging from 6.0 to 6.5, the valence of Cu(II) [Cu on the Cu(II) site] remains $+2$ and that of Cu(I) [Cu on the Cu(I) site] increases. Instead, both valences of Cu(II) and Cu(I) change following the oxygen content between 6.5 and 7.0. Assuming that Brown's result holds also for high temperatures, the numbers of Cu^+, Cu^{2+}, and Cu^{3+} ions in unit cells of the three oxides were calculated on the basis of the chemical equilibrium of defect formation.

(1) Case A ($6.0\leqslant y\leqslant 6.5$). Dissolution of oxygen into oxide results in increasing Cu valence. The reactions are

$$4Cu_A^X+2V_{\ddot{O}}+O_2=4Cu_A^{\cdot}+2O^X, \tag{A1}$$

$$4Cu_A'+2V_{\ddot{O}}+O_2=4Cu_A^X+2O^X, \tag{A2}$$

where Cu_A', Cu_A^X, and $Cu_A^{\cdot}$ denote the Cu^+, Cu^{2+}, and Cu^{3+} ions in the oxide, $V_{\ddot{O}}$ and O^X represent the oxygen vacancy and the oxide ion on the anionic site. The law of mass action, for y between 6.0 and 6.5, provides

$$\frac{[Cu_A^{\cdot}]^4[O^X]^2}{[Cu_A^X]^4[V_{\ddot{O}}]^2P_{O_2}}=K_1, \tag{A3}$$

$$\frac{[Cu_A^X]^4[O^X]^2}{[Cu_A']^4[V_{\ddot{O}}]^2P_{O_2}}=K_2 \tag{A4}$$

where K_1 and K_2 are the equilibrium constants for the reactions (A1) and (A2), and [ ] represents the numbers of ions and defects in unit cells. For y between 6.0 and 6.5, as discussed before, the valence of Cu(II) is $+2$ and is constant, while the valence of Cu(I) increases. The site conservation condition for the Cu(I) site yields

$$[Cu_A']+[Cu_A^X]+[Cu_A^{\cdot}]=1. \tag{A5}$$

For this oxygen content range, $PrBa_2Cu_3O_y$, $Pr_{0.5}Y_{0.5}Ba_2Cu_3O_y$, and $YBa_2Cu_3O_y$ are tetragonal with two oxygen sites per unit cell. Accordingly,

$$[O^X]+[V_{\ddot{O}}]=2, \tag{A6}$$

$$[V_{\ddot{O}}]=1-\delta, \tag{A7}$$

$$[O^X]=1+\delta. \tag{A8}$$

Denoting the average Cu valence by z and the oxygen content by $7-\delta$, and using the condition of electroneutrality, one obtains

$$3z=7-2\delta. \tag{A9}$$

Since the valence of Cu(II) is always $+2$, the valence of Cu(I) is $3z-4$, and

$$3[Cu_A']+2[Cu_A^X]+[Cu_A^{\cdot}]=3-2\delta. \tag{A10}$$

Inserting Eqs. (A6)–(A8) into Eq. (A3) and Eq. (A4), one obtains

$$[Cu_A^{\cdot}]=(K_1\cdot P_{O_2})^{1/4}\left(\frac{1-\delta}{1+\delta}\right)^{1/2}[Cu_A^X], \tag{A11}$$

$$[Cu_A']=(K_2\cdot P_{O_2})^{-1/4}\left(\frac{1-\delta}{1+\delta}\right)^{-1/2}[Cu_A^X]. \tag{A12}$$

Inserting Eq. (A11) and Eq. (A12) into Eq. (A5) and Eq. (A10), one gets

$$\left\{(K_1\cdot P_{O_2})^{1/4}\left(\frac{1-\delta}{1+\delta}\right)^{1/2}+1+(K_2\cdot P_{O_2})^{-1/4}\left(\frac{1-\delta}{1+\delta}\right)^{1/2}\right\}\times[Cu_A^X]=1 \tag{A13}$$

$$\left\{3(K_1\cdot P_{O_2})^{1/4}\left(\frac{1-\delta}{1+\delta}\right)^{1/2}+2+(K_2\cdot P_{O_2})^{-1/4}\left(\frac{1-\delta}{1+\delta}\right)^{1/2}\right\}\times[Cu_A^X]=3-2\delta. \tag{A14}$$

Elimination of $[Cu_A^X]$ from Eq. (A13) and Eq. (A14) provides

$$2\delta(K_1\cdot P_{O_2})^{1/4}\left(\frac{1-\delta}{1+\delta}\right)^{1/2}+(2\delta-1)+(K_2\cdot P_{O_2})^{-1/4}\left(\frac{1-\delta}{1+\delta}\right)^{1/2}=0. \tag{A15}$$

Setting

$$P_{O_2}^{1/4}\left(\frac{1-\delta}{1+\delta}\right)^{1/2}=X, \tag{A16}$$

one obtains the quadratic equation

$$2\delta K_1^{1/4}X^2+(2\delta-1)X+2(\delta-1)K_2^{-1/4}=0 \tag{A17}$$

with the solution

$$X=P_{O_2}^{1/4}\left(\frac{1-\delta}{1+\delta}\right)^{1/2}$$
$$=\frac{-(2\delta-1)+\sqrt{(2\delta-1)^2-16\delta(\delta-1)(K_1/K_2)^{1/4}}}{4\delta K_1{}^{1/4}}. \tag{A18}$$

Equation (A18) gives the relation between the oxygen partial pressure P_{O_2} and the oxygen content $7-\delta$.

(2) Case B ($6.5\leqslant y\leqslant 7.0$). In this case, the crystal structure is orthorhombic, and both Cu(II) and Cu(I) ions have the same valence. The mass action law gives

$$\frac{[Cu_B^{\cdot}]^4[O^X]^2}{[Cu_B^X]^4[V_{\ddot{O}}]^2P_{O_2}}=K_3, \tag{A19}$$

$$\frac{[Cu_B^X]^4[O^X]^2}{[Cu_B]^4[V_{\ddot{O}}]^2P_{O_2}}=K_4, \tag{A20}$$

where Cu_B', Cu_B^X, and $Cu_B^{\cdot}$ are the Cu^+, Cu^{2+}, and Cu^{3+} ions on the Cu(II)-O_2 plane and the Cu(I)-O chain, and K_3 and K_4 are the equilibrium constants. Since there are three Cu ion sites,

$$[Cu_B']+[Cu_B^X]+[Cu_B^{\cdot}]=3. \tag{A21}$$

In the orthorhombic phase, there is only one oxygen ion site per unit cell, and

$$[O^X]+[V_{\ddot{O}}]=1, \tag{A22}$$

$$[V_{\ddot{O}}]=\delta, \tag{A23}$$

$$[O^X]=1-\delta. \tag{A24}$$

TABLE I. Equilibrium constant for the master curve.

Sample	K_1	K_2	K_3	K_4
$PrBa_2Cu_3O_y$	1.3×10^2	6.0×10^{-2}	3.5×10^{-2}	1.4×10^4
$(Pr_{0.5}Y_{0.5})Ba_2Cu_3O_y$	1.2×10^2	3.0×10^{-2}	8.0×10^{-2}	2.2×10^4
$YBa_2Cu_3O_y$	0.9×10^2	1.0×10^{-2}	1.5×10^{-1}	3.5×10^4

The condition of electroneutrality yields

$$3z=7-2\delta. \tag{A25}$$

Therefore,

$$[Cu_B']+2[Cu_B^X]+3[Cu_B^{\cdot}]=7-2\delta. \tag{A26}$$

Inserting Eqs. (A28)–(A30) into Eq. (A25) and Eq. (A26) yields

$$[Cu_B^{\cdot}]=(K_3\cdot P_{O_2})^{1/4}\left(\frac{\delta}{1-\delta}\right)^{1/2}[Cu_B^X], \tag{A27}$$

$$[Cu_B']=(K_4\cdot P_{O_2})^{-1/4}\left(\frac{\delta}{1-\delta}\right)^{-1/2}[Cu_B^X]. \tag{A28}$$

Inserting Eq. (33) and Eq. (34) into Eq. (27) and Eq. (32), and setting

$$P_{O_2}^{1/4}\left(\frac{\delta}{1-\delta}\right)^{1/2}=X \tag{A29}$$

yields

$$X=P_{O_2}^{1/4}\left(\frac{\delta}{1-\delta}\right)^{1/2}$$
$$=\frac{-(2\delta-1)+\sqrt{(2\delta-1)^2-16(\delta+1)(\delta-2)(K_3/K_4)^{1/4}}}{4(\delta+1)K_3^{1/4}}. \tag{A30}$$

The solid lines in Fig. 2 represent the master curves obtained using Eq. (A18) and Eq. (A30). They agree well with the experimental master curves (symbols). The equilibrium constants used for the best fitting to the master curves are listed in Table I.

[1] M. K. Wu, J. R. Ashburn, C. J. Torng, P. H. Hor, R. L. Meng, L. Gao, Z. J. Huang, Y. Q. Wang, and C. W. Chu, Phys. Rev. Lett. **58**, 908 (1987).

[2] L. F. Schneemeyer, J. V. Waszczak, S. M. Zahorac, R. B. van Dover, and T. Siegrist, Mater. Res. Bull. **22**, 1467 (1987).

[3] E. M. Engler, V. Y. Lee, A. I. Nassal, R. B. Beyers, G. Lim, P. M. Grant, S. S. P. Parkin, M. L. Ramirez, J. E. Vazquez, and R. J. Savoy, J. Am. Chem. Soc. **109**, 2848 (1987).

[4] A. Hartmann and G. J. Russell, Solid State Commun. **95**, 791 (1995).

[5] C. A. Draxl, P. Blaha, and K. Schwarz, J. Phys., Condens. Matter. **6**, 2347 (1994).

[6] Y. H. Ko, H. K. Kweon, H. C. Lee, and N. H. Hur, Physica C **224**, 357 (1994).

[7] P. Xiong, G. Xiao, and X. D. Wu, Phys. Rev. B **47**, 5516 (1993).

[8] H. Iwasaki, J. Sugawara, and N. Kobayashi, Physica C **185-189**, 1249 (1991).

[9] O. E. Parfionov and A. A. Konovalov, Physica C **202**, 385 (1992).

[10] K. Takita and T. Ohshima, Physica C **185-189**, 757 (1991).

[11] C. K. Lowe-ma and T. A. Vanderah, Physica C **201**, 233 (1992).

[12] Y. Dalichaouch, M. S. Torikachvili, E. A. Early, B. W. Lee, C. L. Seaman, K. N. Yang, H. Zhou, and M. B. Maple, Solid State Commun. **65**, 1001 (1988).

[13] U. Neukirch, C. T. Simmons, P. Sladeczek, C. Laubschat, O. Strebel, G. Kaindl, and D. D. Sarma, Europhys. Lett. **5**, 567 (1988).

[14] J. Fink, N. Nucker, H. Romberg, M. Alexander, M. B. Maple, J. J. Neumeier, and J. W. Allen, Phys. Rev. B **42**, 4823 (1990).

[15] H. B. Radousky, J. Mater. Res. **7**, 1917 (1992).

[16] M. B. Maple, B. W. Lee, J. J. Neumeier, G. Nieva, L. M. Paulius,

and C. L. Seaman, J. Alloys Compd. **181**, 135 (1992).
[17] L. Soderholm and G. L. Goodman, J. Solid State Chem. **81**, 121 (1989).
[18] L. Soderholm, G. L. Goodman, and C.-K. Loong, J. Appl. Phys. **67**, 5067 (1990).
[19] G. L. Goodman, C.-K. Loong, and L. Soderholm, J. Phys., Condens. Matter. **3**, 49 (1991).
[20] H.-D. Jostarndt, U. Walter, J. Harnischmacher, J. Kalenborn, A. Severing, and E. Holland-Moritz, Phys. Rev. B **46**, 14 872 (1992).
[21] Y. Idemoto, Y. Yasuda, and K. Fueki, Physica C **243**, 35 (1995).
[22] Y. Idemoto, H. Tokue, and K. Fueki, Physica C **243**, 43 (1995).
[23] M. Namiki and K. Hirokawa, J. Anal. Chem. USSR **1**, 1 (1992).
[24] K. Kishio, J. Shimoyama, T. Hasegawa, K. Kitazawa, and K. Fueki, Jpn. J. Appl. Phys. **26**, L1228 (1987).
[25] K. Kishio, T. Hasegawa, K. Suzuki, K. Kitazawa, and K. Fueki, in *High-Temperature Superconductors: Relationships Between Properties, Structure, and Solid-State Chemistry*, edited by J. R. Jorgensen *et al.*, MRS Symposia Proceedings No. 156 (Materials Research Society, Pittsburgh, 1989), p. 91.
[26] Y. Kubo, Y. Nakabayashi, J. Tabuchi, T. Yoshitake, A. Ochi, K. Utsumi, H. Igarashi, and M. Yonezawa, Jpn. J. Appl. Phys. **26**, L1888 (1987).
[27] P. Strobel, J. J. Capponi, M. Marezio, and P. Monod, Solid State Commun. **64**, 513 (1987).
[28] T. B. Lindemer and E. D. Specht, Physica C **268**, 271 (1996).
[29] Y. Idemoto and K. Fueki, Jpn. J. Appl. Phys. **29**, 2725 (1990).
[30] H. Ishizuka, Y. Idemoto, and K. Fueki, Physica C **195**, 145 (1992).
[31] I. D. Brown, J. Solid State Chem. **82**, 122 (1989).
[32] K. Fueki and Y. Idemoto, in *Defects in Materials*, edited by P. D. Binstowe *et al.*, MRS Symposia Proceedings No. 209 (Materials Research Society, Pittsburgh, 1991), p. 783.
[33] Y. Idemoto and K. Fueki, Jpn. J. Appl. Phys. **30**, 2471 (1991).
[34] Y. Idemoto, S. Fujiwara, and K. Fueki, Physica C **179**, 96 (1991).
[35] Y. Idemoto, S. Fujiwara, and K. Fueki, Physica C **176**, 325 (1991).
[36] Y. Idemoto and K. Fueki, Physica C **190**, 502 (1992).
[37] Y. Idemoto, Y. Itoh, and K. Fueki, Physica C **202**, 127 (1992).
[38] H. Ishizuka, Y. Idemoto, and K. Fueki, Physica C **204**, 55 (1992).
[39] Y. Idemoto, T. Muroga, and K. Fueki, Physica C **210**, 315 (1993).
[40] Y. Idemoto, H. Tokunaga, and K. Fueki, Physica C **231**, 37 (1994).
[41] Y. Idemoto, T. Toda, and K. Fueki, Physica C **249**, 123 (1995).
[42] I. A. Leonidov, Ya. N. Blinovskov, E. E. Flyatau, P. Ya. Novak, and V. L. Kozhevnikov, Physica C **158**, 287 (1989).
[43] G. Sageev Grader, P. K. Gallagher, and E. M. Gyorgy, Appl. Phys. Lett. **51**, 1115 (1987).
[44] Han-III Yoo and Sang-Min Lee, J. Am. Ceram. Soc. **77**, 3131 (1994).
[45] B. Fisher, E. Polturak, G. Koren, A. Kessel, R. Fischer, and L. Harel, Solid State Commun. **64**, 87 (1987).
[46] P. P. Fritas and T. S. Plaskett, Phys. Rev. B **36**, 5723 (1987).
[47] M. Gurvitch and A. T. Fiory, Phys. Rev. Lett. **59**, 1337 (1987).
[48] I. A. Leonidov, Ya. N. Blinovskov, E. E. Flyatau, P. Ya. Novak, and V. L. Kozhevnikov, Physica C **158**, 287 (1989).
[49] P. P. Freitas and T. S. Plaskett, Phys. Rev. B **36**, 5723 (1987).
[50] P. P. Freitas and T. S. Plaskett, Phys. Rev. B **37**, 3657 (1988).
[51] J. D. Jorgensen, M. A. Beno, D. G. Hinks, L. Soderholm, K. J. Volin, R. L. Hitterman, J. D. Grace, Ivan K. Schuller, C. U. Segre, K. Zhang, and M. S. Kleefisch, Phys. Rev. B **36**, 3608 (1987).
[52] H. Yoo and H. Choi, J. Am. Ceram. Soc. **75**, 2707 (1992).
[53] V. E. Zubkus, O. E. Parfionov, E. E. Tornau, and P. J. Kundrotas, Physica C **198**, 141 (1992).
[54] J. R. Cooper, S. D. Obertelli, A. Carrington, and J. W. Loran, Phys. Rev. B **44**, 12 086 (1991).
[55] E. C. Jones, D. K. Christen, J. R. Thompson, R. Feenstra, S. Zhu, D. H. Lowndes, Julia M. Phillips, M. P. Siegal, and J. D. Budai, Phys. Rev. B **47**, 8986 (1993).
[56] K. Kallias, I. Panagiotopoulos, D. Niarchos, and A. Kostikas, Phys. Rev. B **48**, 15 992 (1993).
[57] H.-I. Yoo and S.-M. Le, J. Am. Ceram. Soc. **77**, 3131 (1994).
[58] O. E. Parfionov and A. A. Konovalov, Physica C **202**, 385 (1992).
[59] H. Yasuoka, H. Mazaki, T. Terashima, and Y. Bando, Physica C **175**, 192 (1991).
[60] I. Ya. Fugol, V. N. Samovarov, Yu. I. Rybalko, and V. M. Zhuravlev, J. Mod. Phys. B **6**, 1475 (1992).
[61] S. Uchida, T. Ido, H. Takagi, T. Arima, Y. Tokura, and S. Tajima, Phys. Rev. B **43**, 7942 (1991).
[62] S. Uchida., H. Takagi, and Y. Tokura, Physica C **162-164**, 1677 (1989).
[63] J. M. Ginder, M. G. Roe, Y. Song, R. P. McCall, J. R. Gaines, E. Ehrenfreund, and A. J. Epstein, Phys. Rev. B **37**, 7506 (1988).
[64] M. Suzuki Phys. Rev. B **39**, 2312 (1989).
[65] M. Sato, R. Horiba, and K. Nagasaka, Phys. Rev. Lett. **22**, 1175 (1993).
[66] O. T. Sorensen, *Nonstoichiometric Oxides* (Academic, London, 1981), p. 300.
[67] S. Uchida, T. Ido, H. Takagi, T. Arima, Y. Tokura, and S. Tajima, Phys. Rev. B **43**, 7942 (1991).